International Journal of Terrestrial Heat Flow and Applied Geothermics
VOL. 3, NO. 1 (2020); P. 01-10.
ISSN: 2595-4180
DOI: https://doi.org/10.31214/ijthfa.v3i1.51

IJTHFA
http://ijthfa.com/

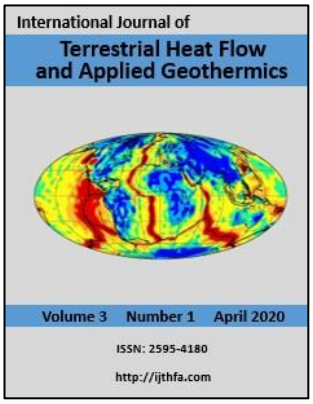

Heat flow variations in the Antarctic Continent

Suze Nei P. Guimarães, Fábio P. Vieira, Valiya M. Hamza
[1] Department of Geophysics, National Observatory, Rio de Janeiro, Brazil.

Email address
suze@on.br (S.N.P. Guimarães)
Corresponding author

Abstract

The present work provides a reappraisal of terrestrial heat flow variations in the Antarctic continent, based on recent advances in data analysis and regional assessments. The data considered include those reported at the website of IHFC and 78 additional sites where measurements have been made using a variety of techniques. These include values based on the Method of Magmatic Heat Budget (MHB) for 41 localities in areas of recent volcanic activity and estimates that rely on basal temperatures of glaciers in 372 localities that are known to host subglacial lakes. The total number of data assembled is 491, which has been useful in deriving a 10^{o}x10^{o} grid system of homogenized heat flow values and in deriving a new heat flow map of the Antarctic continent. The results reveal that the Antarctic Peninsula and western segment of the Antarctic continent has distinctly high heat flow relative to the eastern regions. The general pattern of differences in heat flow between eastern and western of Antarctic continent is in striking agreement with results based on seismic velocities.

Keywords
Terrestrial Heat Flow
Antarctic Continent

Received: December 5, 2019

Accepted: February 10, 2020

Published: April 01, 2020

1. Introduction

It is widely recognized that heat flux from the Earth's interior is a significant source of thermal energy in Polar Regions. Detailed understanding subglacial geothermal field beneath Antarctic ice sheet is important not only for outlining crustal geothermal conditions but also for understanding deep tectonic processes. Results of early geophysical studies reveal that much of the Antarctic region is below sea level, a consequence of isostatic adjustment of local crust in response to the weight of ice cap. It is bounded by extensional mid-ocean ridge systems. The present adjoining lithospheric segments are Nazca, South America, Africa, Somalia, Australia and Pacific. Figure 1 illustrates the current locations of these plates relative to the Antarctic continent. Note that the upper plate segment of Antarctic Peninsula is in contact with southwestern segment of the South American plate.

The current understanding of rocks and geological structures in Antarctic region beneath the ice have been inferred from the limited areas exposed at the surface as well as from remote sensing technologies that include satellite imagery, ground penetrating radar, use of seismic waves, and study of gravity anomalies. Very little is known of regional heat flow variations within the Antarctic plate segment and its interactions with the geothermal fields of neighbouring tectonic units. A number of geothermal studies have been carried out in the Antarctic region. We mention here a selected list of works by Risk and Hochstein (1974), Engelhardt (2004), Morin et al. (2010), Carson et al. (2014), Schroeder et al. (2014), Fischer et al. (2015), Begelman et al. (2017), Dziadek et al. (2017). One of the convenient ways of minimizing such limitations is to make use of results of suitable geophysical surveys that can provide proxy information useful for assessment of subsurface thermal conditions. In particular, appropriate geophysical survey data on thickness and basal temperatures of glaciers in areas of subglacial lakes may be employed as proxy for estimating regional scale variations in heat flow across Antarctica. This is the approach adopted in the present work.

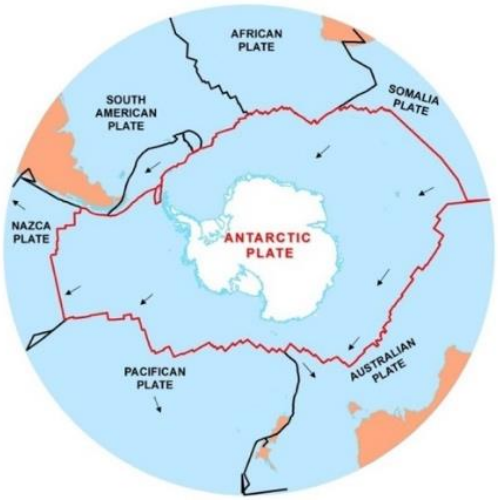

Figure 1 – Antarctic lithospheric segment and adjoining plates. The curve in red color indicates plate boundaries. The arrows indicate directions of plate movement. (Adapted with modifications from EarhHow, 2019).

2. Geologic Context of the Study Area

The Antarctic region may be divided into two distinct geological provinces, separated by the Transantarctic Mountains (see for example Harley et al, 2013). The eastern segment is dominated by cratonic igneous and metamorphic rocks of Precambrian age. Exposures have been mapped along the coast and inland localities, as described in studies of Fedorov et al, (1982), Lisker et al (2003), and Phillips and Laufer (2009). The Transantarctic Mountains is located along the Neoproterozoic passive margin on the edge of the East Antarctic Craton. According to Stump (1995) and Goodge (2002) it had transformed into an active convergent margin by the Cambro-Ordovician period. Prominent features of East Antarctica include the Transantarctic Mountains, Gamburtsev Mountains, Vostok Highlands, Dronning Maud Land, Prince Charles Mountains, Lambert Graben, Amery Shelf, Prydz and Lutzow–Holm bays, Lake Vostok as well as Aurora and Wilkes basins.

On the other hand, West Antarctica comprises several Palaeozoic–Mesozoic terranes dominated by magmatic arc systems. According to Dalziel and Elliot (1982) and Vaughan et al, (2005) these have been subject to active tectonic processes during the Palaeozoic and Mesozoic. Principal blocks of West Antarctica include the Antarctic Peninsula, the Ellsworth–Whitmore Block, Haag Nunataks, Marie Byrd Land, and the Thurston Block.

3. Geothermal data sets

In the present work, we consider heat flow data sets available as parts of global compilations of IHFC, inferred values based on present knowledge of the magmatic heat budget of volcanic settings and estimates that rely on basal temperatures of glaciers in localities which are known to host subglacial lakes. Notable in this context are large data sets derived from basal temperatures and thicknesses of frozen layers that allowed estimates of heat flow in areas of approximately 400 subglacial lakes, distributed mainly in the eastern parts of Antarctica (See for example: Robin et al., 1970; Siegert et al., 2005; Wright and Siegert, 2012).

3.1. Heat Flow Data Reported in Previous Works

As per the website maintained by the International Heat Flow Commission (IHFC, 2009) heat flow values have been reported for 8 localities of the Antarctic continent. The earlier IHFC website is currently inactive. In a more recent work, Martos et al. (2017) reported heat flow values for additional 29 sites. A summary of data reported in these compilations is presented in Table 1. Both compilations have been edited for completing some of the missing details and in eliminating duplicate data. In the case of IHFC data, heat flow in excess of 100 mW/m^2 has been reported for North Fork basin and Lake Leon. The remaining sites have moderate to low heat flow. In the case of data set reported by Martos et al (2017) values in excess of 150 mW/m^2 has been reported for Lake Whillans, West Antarctic ice sheet and Hut Point Peninsula (Ross Island). Intermediate heat flow in the range of 80 to 120 mW/m2 have been reported for 11 sites. Heat flow in excess of global mean value of 65mW/m^2 (Vieira and Hamza, 2018) has been found for 6 localities in IHFC compilation and 19 localities in the data set of Martos et al. (2017). Most of high heat flow values (>65mW/m^2) are found to occur in west Antarctic region. Relatively low values are found in localities of the east Antarctic region.

Table 1 –Locations and heat flux (q in mW/m^2) values of data sets for Antarctica reported in previous compilations.

Locality	Longitude (degree)	Latitude (degree)	q
DVDP-14/North Fork	161.41	-77.54	142
DVDP-12/Lake Leon	162.85	-77.63	100
DVDP-3/Ross Island	166.67	-77.85	92
DVDP-6/Lake Vida	161.81	-77.38	88
DVDP-3/Ross Island	166.67	-77.85	84
DVDP-3/Ross Island	166.67	-77.85	75
Nagursk-1	47.71	-80.78	57
Nagursk-1.2	-168.62	-88.37	54
Lake Whillans	206.31	-84.24	285
WA Ice Sheet	-112.09	-79.49	240
Hut Point (Ross Isl.)	166.67	-77.82	164
McMurdo	162.28	-77.76	115
Thwaites Glacier WA	106.80	-75.50	114
Lake Whillans	206.310	-84.24	105
Concordia Subglacial	125.050	-74.05	100
Dolleman Island	-60.930	-70.58	100
Dyer Plateau	-65.000	-70.50	100
Thwaites Glacier WA	106.80	-75.50	97
Siple Coast	-155.00	-82.00	90
Bruce Plateau	-64.07	-66.03	87
Lake Vida	161.81	-77.82	85
McMurdo Ice Shelf	162.28	-77.76	82
Byrd Station	-119.52	-80.01	75
Law Dome	112.80	-66.76	75
Siple Dome	-148.81	-81.65	69
EPICA Dome C	123.40	-75.10	67
Southern Prydz Bay	76.00	-69.50	65
Upper Vincennes	122.00	-73.50	65
South Pole	0.00	-90.00	61
Dome F	39.70	-75.10	59
Vostok	106.87	-78.45	53
EPICA Dome C	123.40	-75.10	45
Conc. Trench Dome C	125.05	-74.05	40
Dome C area	123.83	-75.12	40
Lower Vincennes	122.00	-73.50	40
Rauer Islands	77.83	-68.85	40
Vestfold Hills Block	78.25	-68.68	31

3.2. Estimates of Heat Flow for Volcanic Regions

In west Antarctic, there are two major volcanic environments, namely West Antarctic rift system and its associated alkaline provinces, and the volcanic field of northern Antarctic Peninsula. In nearby oceanic regions and in basins surrounding Antarctica there are several intraplate island volcanoes, as for example the active South Sandwich island arc. During post-Cretaceous times, there has been uplift and rifting between West and East Antarctica. The rift system in western segment is still active and hosts much of current volcanic activity in Antarctica. There are also inactive volcanoes in the Transantarctic Mountains. Figure 2 indicates locations of main volcanic systems in the Antarctic region (LeMasurier, et al. 1990).

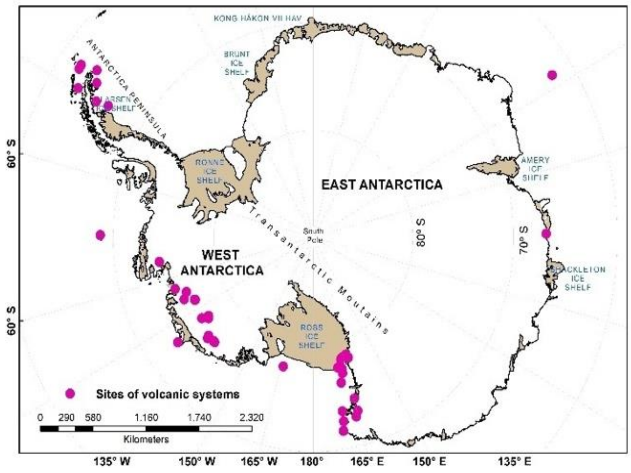

A list of regions of volcanic activity where residual heat is important may be considered is given in Table 2. Note that most of the volcanic systems are located in west Antarctic region, to the southwest of the Transantarctic Mountains. Areas of recent volcanism are absent in east Antarctica, located to the northeast of this mountain system.

Table 2 – Regions of recent volcanism in Antarctic Peninsula. Alt. – Altitude (m); E_{te}–Estimate of time elapsed since latest magma activity.

Locality	Alt.	Longitude (degree)	Latitude (degree)	E_{te} (Yrs)
Mount Berlin	3478	-134.13	-76.05	<100
Mount Erebus	3794	167.15	-77.52	<100
Brown Peak	1167	164.58	-67.42	<100
Deception Is.	602	-59.37	-62.95	<100
Penguin Island	180	-56.10	-62.10	<100
Mt. Melbourne	2732	164.70	-74.35	<100
L. Christiansen	1640	-89.48	-68.77	<200
Paulet Island	353	-54.22	-63.58	1000
Hudson Mount.	749	-98.50	-74.42	2230
The Pleiades	3040	165.53	-72.70	3070
Mt. Haddington	1630	-56.37	-64.22	5000
Mount Takahe	3460	-111.92	-76.28	7570
Mt. Waesche	3292	-125.10	-77.17	8000
Melville Peak	549	57.68	-62.02	11700
Mount Siple	3110	-125.90	-73.25	19500
R. Soc. Range	3000	162.67	-78.17	80000
Mount Andrus	2978	-131.77	-75.80	100000
Seal Nunatak	368	-59.70	-65.05	200000
Mt. Morning	2723	163.58	-78.52	200000
Mount Bursey	2787	-131.37	-76.02	490000
Mount Moulton	3070	-134.87	-76.05	480000
Toney Mt.	3595	-114.20	-75.80	500000
Mt.Terra Nova	2130	-166.05	-77.52	800000
Mount Terror	3262	168.53	-77.52	820000
Mount Murphy	2703	-109.27	-75.33	900000
Argo Point	360	-59.08	-66.25	900000
Beaufort Island	740	166.93	-76.93	1.3×10^6
Bridgeman Is.	240	-55.27	-62.07	1.3×10^6
Black Island	1041	166.42	-78.20	1.7×10^6
Mount Frakes	3654	-116.30	-76.80	1.7×10^6
Mt. Discovery	2578	165.02	-78.37	1.9×10^6
Franklin Island	247	168.32	-76.08	2.6×10^6
Adare Penin.	2083	170.50	-71.67	2.6×10^6
Gaussberg	370	89.18	-66.80	2.6×10^6
Mount Bird	1765	166.73	-77.27	$3.8\text{-}4.6 \times 10^6$
Mount Sidley	4285	-125.90	-77.03	4.7×10^6
Mount Harcourt	1570	169.92	-72.53	5.5×10^6
Mount Overlord	3395	164.60	-73.17	7.0×10^6
Coulman Island	1,998	169.75	-73.47	7.2×10^6
Mount Steere	3500	-116.18	-76.73	8.0×10^6
Mt. Hampton	3325	-124.20	-76.48	11×10^6

According to available information (see for example, Harley et al., 2013) most of the recent volcanic activities in western parts of Antarctica have age values less than a few thousand years while the volumes of magma chambers emplaced are in the range of 10^2 to 10^4 km^3.

Our interest in the present context is in estimating heat flux for volcanic regions in the Antarctic. The starting point is the relation between magma volume (in cubic kilometers) and time elapsed (in years) proposed by Smith and Shaw (1978). It is approximately linear, when both are expressed on log scale.

An example of this line of reasoning is illustrated in Figure 3 where the domain limited by dashed lines may be considered as representing the extent of regions where residual heat is important. It includes west Antarctic Peninsula and regions of transantarctic rift system. In other words, sites falling in the region below the belt of dotted lines may be considered as having potential for retaining residual magmatic heat in subsurface layers. For the same reason, sites falling above the belt of dotted lines may be considered as those with little residual magmatic heat.

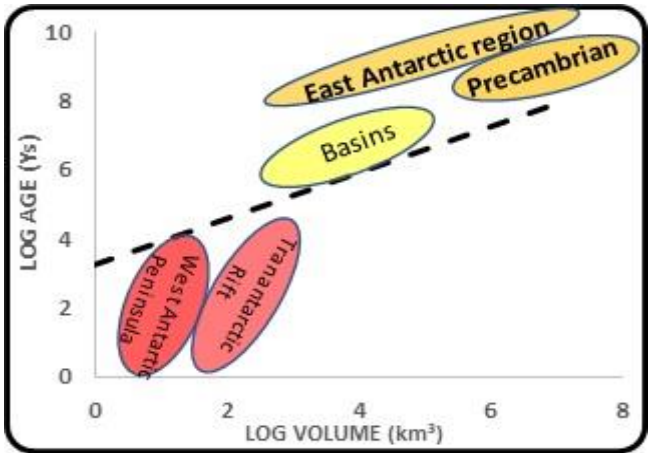

Figure 3 – Relation between magma volume and elapsed time of volcanic activity for the Antarctic continent.

According to Noguchi (1970), Annen et al. (2006) and Suarez (2017) the emplacement temperature of andesitic magma at mid crustal levels is approximately 1200ºC while the depth of emplacement falls mostly in the range of 10 to 15 km. For the purposes of the present work, a mean depth value of 12.5 ± 2.5 km has been assumed for all areas of recent volcanism. This is obviously a first order simplification, which can be improved with availability of more reliable data. Noguchi (1970) argued that magma temperatures drop to about 900ºC in about 60000 years after emplacement. This argument allows intra-crustal magma chamber emplacement temperature (T_e) to be estimated from the elapsed time of emplacement (a_e). For the age range of 0 to 60000 years, the relation is:

$$T_{emp} = 1200 - (300/60000)a_e \qquad (1)$$

In this case, a_e is equivalent of E_{te} in table 2. For times greater than 60000 years, the magma temperature is assumed to drop to about 500ºC. The arguments of Noguchi (1970), Annen et al (2006) and Suarez (2017) are based on petrological considerations and is equivalent to the simplified assumption that temperature gradient in the crust, above regions of magma emplacement, falls from the initial value of about 95ºC/km to about 75ºC/km in 60000 years. These are

obviously first order estimates but considered sufficient for describing main heat flow variations in regions of deep-seated magma intrusions.

The next step is determination of heat flow corresponding to the emplacement temperature (Te). For a crust with temperature dependent thermal conductivity (λ), the relevant relation for magmatic heat flow (q_e) corresponding to residual temperature (Te) as a function of depth (z) is (Carslaw and Jaeger, 1959; Iyer and Hamza, 2019):

$$q_e(z) = \frac{\lambda_0}{z_s \alpha} \ln\left(\frac{\theta_m}{\theta_0}\right) \qquad (2)$$

where $\theta_m = 1 + \alpha T_e$ and $\theta_0 = 1 + \alpha T_0$, α is the temperature coefficient of thermal conductivity and T_0 the surface temperature. This approach of estimating heat flow for volcanic regions has been designated as the method of magmatic heat budget – MHB by Vieira and Hamza (2019). The values of parameter adopted in the MHB method for selected areas of recent volcanism in the Antarctic Peninsula are given in Table 3 for 41 sites.

Table 3 –Values adopted in applying MHB method for estimating heat flow in areas of recent volcanism in the Antarctic Peninsula.

Volcanic Structure	t_e (Yrs)	T_m (°C)	q (mW/m²)
Mount Berlin	<100	1200	180 - 220
Mount Erebus	<100	1200	180 - 220
Brown Peak	<100	1200	180 - 220
Deception Is.	<100	1200	180 - 220
Penguin Island	<100	1200	180 - 220
Mt. Melbourne	<100	1200	180 - 220
L. Christiansen	<200	1199	170 - 210
Paulet Island	1000	1195	170 - 210
Hudson Mount.	2230	1189	170 - 210
The Pleiades	3070	1185	170 - 210
Mt. Haddington	5000	1175	160 - 200
Mount Takahe	7570	1162	160 - 200
Mt. Waesche	8000	1160	160 - 200
Melville Peak	11700	1142	160 - 200
Mount Siple	19500	1103	160 - 200
R. Soc. Range	80000	800	120 - 160
Mount Andrus	100000	700	120 - 160
Seal Nunatak	200000	500	80 - 100
Mt. Morning	200000	500	80 - 100
Mount Bursey	490000	500	80 - 100
Mount Moulton	480000	500	80 - 100
Toney Mt.	500000	500	80 - 100
Mt.Terra Nova	800000	500	80 - 100
Mount Terror	820000	500	80 - 100
Mount Murphy	900000	500	80 - 100
Argo Point	900000	500	80 - 100
Beaufort Island	1.3×10^6	500	60 - 80
Bridgeman Is.	1.3×10^6	500	60 - 80
Black Island	1.7×10^6	500	60 - 80
Mount Frakes	1.7×10^6	500	60 - 80
Mt. Discovery	1.9×10^6	500	60 - 80
Franklin Island	2.6×10^6	500	60 - 80
Adare Penin.	2.6×10^6	500	60 - 80
Gaussberg	2.6×10^6	500	60 - 80
Mount Bird	3.8×10^6	500	60 - 80
Mount Sidley	4.7×10^6	500	60 - 80
Mount Harcourt	5.5×10^6	500	60 - 80
Mount Overlord	7.0×10^6	500	60 - 80
Coulman Island	7.2×10^6	500	60 - 80
Mount Steere	8.0×10^6	500	60 - 80
Mt. Hampton	11×10^6	500	60 - 80

The subscript zero in equation (2) indicate values of parameters evaluated at the surface (z = 0; T_0 = 0). These calculations assume a mean value of 0.0011 for temperature coefficient of thermal conductivity (α) and a mean thermal conductivity (λ_0) of 2 W/m/K for basic magmatic rocks.

The limitations in the arguments of Noguchi (1970) and Smith and Shaw (1978) impose constraints on the validity of Eq. (2). Thus, heat flow values obtained using this approach should only be considered as first order approximations, useful for initial estimates of heat flow in areas of recent magmatic activity. On the other hand, such limitations are considered to be of minor importance in the present context of heat flow variations for the Antarctic continent.

Note that we have ignored the contribution of radiogenic heat, as it is only of secondary importance in the present context. For values of time elapsed larger than 60000 years it is assumed that the emplacement temperature of magma drops to about 500°C at depths of 12.5km, which imply a heat flow of 80mW/m².

3.3. Heat Flow estimates for Subglacial Lakes

One of the striking features of the Antarctic region is the presence of a large number of lakes beneath the glaciers (See for example: Robin et al., 1970; Siegert et al., 2005; Wright and Siegert, 2012). Subglacial lakes are bodies of liquid water that lie beneath the ice sheet, at the interface between the ice and the bedrocks. With ice acting as an insulator, typical levels of geothermal heat flux are sufficient to warm the ice base to the pressure melting point, even though surface temperatures are tens of centigrade below freezing. Subglacial water accumulations are under the combined forces of gravity and pressure of the ice above and can promote formations of ponds in subglacial hollows and troughs, forming lakes.

About 372 subglacial lakes has been mapped beneath the Antarctic ice sheets. These range from giant stable lakes to small pockets of water connected with fast-flowing ice streams (Wright and Siegert, 2012). The map of Figure 4 illustrates its spatial distribution.

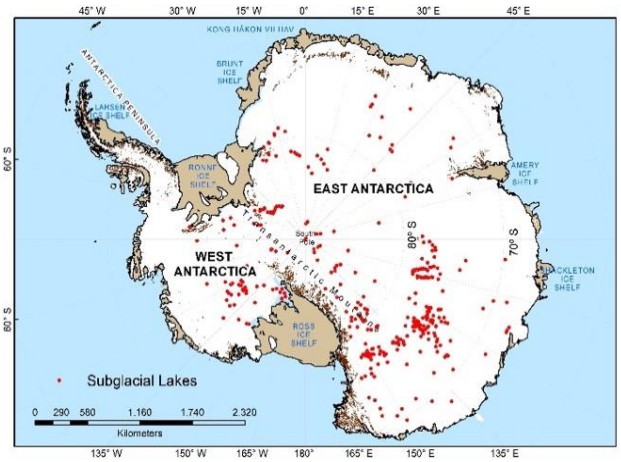

Figure 4 – Map illustrating locations of subglacial lakes (red dots) in the Antarctic continent for which heat flow estimates were made.

In the present work, the focus is on exploring thermal consequences of melting in isolated localities and its application for determining heat flux beneath ice sheets in Antarctic. A number of parameters control basal ice-sheet temperatures. These include ice thickness, surface

temperature, ice accumulation rate and heat transported by horizontal advection. The basal heat gradient is related to the geothermal heat flux, heat produced from basal sliding and heat derived from internal ice deformation.

In models of basal thermal regimes of glaciers, it is customary to take into account the roles of geothermal heat flux, generation of frictional or strain heat near the base of the ice and the temperature changes arising from the height changes of the ice in the surface layer. The basal heating provides the boundary condition for conventional steady-state conditions in which the temperature does not vary with time at a given level in a vertical column through the ice sheet.

The basal thermal gradient is dependent on flow at the ice-sheet base, and its magnitude will therefore increase with distance from the ice divide as glacier velocity increases. However, at the ice divide, the sole supply of basal heat will be from geothermal processes. Numerical models of the ice-sheet thermal regime in such regions have been employed in estimating thermal energy required to allow basal melting to take place.

An analytical model that can be used for such a purpose was developed by Robin (1955) according to which the ratio of basal temperature of the glacier (T_b) and the mean annual surface temperature (T_s) may be written as:

$$\frac{T_b}{T_s} = 1 - \sqrt{\frac{\pi}{2}}\frac{L}{T_s}\left(\frac{dT}{dz}\right)_b \operatorname{erf}\left(\frac{h}{L}\right) \quad (3)$$

In equation (3) z is the vertical coordinate (positive upwards and zero at the ice-sheet base), h is the ice thickness above the sub-glacial lake, b the mean annual surface accumulation of ice-sheet above the lake. The parameter L in Eq. (3) is given by the relation:

$$L = \sqrt{\frac{2\,\lambda\,h}{b}} \text{ and } \left(\frac{dT}{dz}\right)_b = -\frac{q}{\lambda} \quad (4)$$

where α is thermal diffusivity of ice, λ its thermal conductivity and q basal geothermal heat flux and erf the error function (for tabulated values see Carslaw and Jaeger, 1959). The relation for heat flow may be derived from (3) and (4):

$$q = \lambda\,\frac{2\,(T_b - T_s)\sqrt{P/2}}{h\,\sqrt{\pi}\,erf(P/2)} \quad (5)$$

The parameter P in Eq. (5) is the ratio of advection to conduction (known as the Peclet number). It may be expressed as:

$$P = \frac{bh}{\alpha} \quad (6)$$

where b is the accumulation rate of ice. Equation (5) was used in calculating heat flow values making use of estimates of basal temperatures for 372 subglacial lakes. Heat flow higher than 100 mW/m^2 has been found for 11 of the lakes.

In most of the sites in East Antarctic region heat flow values are less than the global mean of 65 mW/m^2 (Vieira and Hamza, 2018). However, there are several localities, mainly in West Antarctic where the heat flow is higher than the global mean. A list of such relatively high heat flow values for 66 sites is presented in Table 4.

Such high values have been considered as arising from hidden geothermal manifestations in subglacial lakes.

Detailed list of heat flow values for the remaining 306 sites is presented in the Appendix.

Table 4 – Subglacial lakes where heat flow is greater than 65mW/m^2. GT – Glacier thickness; q – basal heat flux.

Locality	Longitude (degree)	Latitude (degree)	GT (m)	q (mW/m^2)
Siessor1	334.73	-80.04	293	176
Recovery3	335.88	-80.91	581	124
Recovery1	330.92	-81.15	638	118
Whillans1	202.58	-83.73	638	118
Recovery2	332.83	-81.32	695	113
Whillans2a	199.73	-84.03	759	108
Whillans2b	201.80	-84.34	763	108
Whillans3	206.30	-84.24	798	106
Mercer1	205.81	-84.60	839	103
Whillans4	211.28	-84.37	886	100
Whillans5	213.93	-84.09	895	100
Kamb trunk1	219.59	-81.95	930	98
MacAyeal1	214.64	-79.95	994	95
Slessor3	338.64	-79.92	1032	93
MacAyeal2	215.92	-79.83	1019	93
Whillans7	226.99	-83.24	1047	92
PPT-4	-150.46	-85.21	1086	90
PPT-9	-150.79	-84.90	1094	90
PPT-6	-149.74	-85.16	1134	88
PPT-16	-149.68	-84.66	1149	88
PPT-33	-143.12	-84.77	1150	88
Mac5	220.89	-79.64	1141	88
Rutford1	275.83	-78.18	1151	88
PPT-7	-144.79	-85.08	1157	87
Academy1	298.66	-84.13	1194	86
Foundation1	286.34	-84.52	1197	86
PPT-11	-150.00	-84.75	1219	85
L-King1	157.12	-84.77	1217	85
Raymond1	231.56	-81.35	1296	83
Recovery4	339.95	-81.32	1320	82
Academy3	300.92	-84.61	1357	81
Whillans6	223.09	-83.85	1358	81
Kamb1	228.79	-82.01	1396	80
ByrdS1	152.19	-80.34	1423	79
Slessor2	338.43	-79.84	1404	79
ByrdS3	149.61	-81.80	1433	78
InstituteW2	276.42	-81.63	1495	77
Foundation3	287.21	-85.26	1601	74
PPT-15	-144.12	-84.87	1654	73
Kamb3	231.40	-81.94	1653	73
Kamb2	230.16	-82.18	1709	72
Academy2	302.55	-84.54	1700	72
Kamb4	232.56	-81.97	1755	71
Kamb5	232.52	-82.27	1748	71
M-3809	58.79	-72.78	1750	71
InstituteW1	282.45	-81.40	1754	71
PPT-8	-141.81	-84.97	1801	70
Foundation2	286.03	-84.98	1777	70
David1	157.21	-75.27	1820	70
BindSc1	228.50	-80.35	1855	69
Academy6	304.78	-85.31	1832	69
Slessor4	342.91	-79.34	1847	69
BindSc1	228.50	-80.35	1855	69
Slessor6	345.70	-78.77	1904	68
ByrdS2	149.53	-80.76	1903	68
Lambert1	68.28	-74.00	1873	68
Kamb8	236.86	-82.38	1971	67
Nimrod1	150.28	-83.49	1980	67
Academy4	304.27	-84.81	1955	67
David2	155.52	-75.33	1933	67
Academy5	306.30	-84.84	1972	67
Slessor7	348.95	-79.25	1976	67
Byrd1	148.30	-81.03	2032	66
SI-45	154.13	-79.43	2036	66
InstituteE2	280.99	-82.62	2044	66
Slessor5	342.96	-79.20	2022	66
Academy7	306.28	-85.57	2010	66
Kamb9	238.37	-82.32	2019	66
Kamb6	235.66	-82.06	2097	65

4. New Heat Flow Map of Antarctic Continent

Heat flow data sets discussed in items (2.1), (2.2) and (2.3) were employed in deriving a new heat flow map of the Antarctic continent. Standard mapping procedures adopted for this purpose included calculation of mean heat flow values for a regular grid system of 10 x10 degrees. However, the fact that not all grid elements have observational data creates a problem in interpolation schemes employed for deriving maps. Thus, representative heat flow values derived from the work of Goodge (2018) were assigned for grid elements that did not have observational data.

Note that the work of Goodge (2018) is based on a model of Van Liefferinge and Pattyn (2013), which averages heat flow values derived from various geophysical data sets such as seismic and satellite magnetic data. The overall geographic disposition of data sets compiled in the present work is illustrated in the map of Figure 5. In this map black circles indicate locations of heat flow values based on basal temperatures of subglacial lakes while the red circles indicate those based on the MHB method.

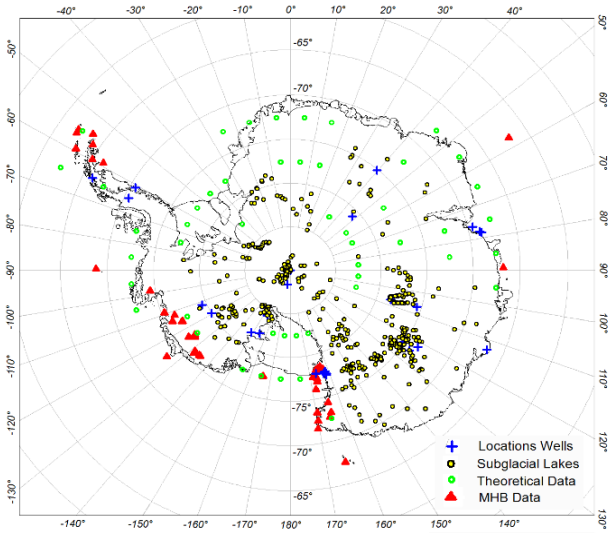

Figure 5 – Locations of heat flow data considered in the present work. The color scheme indicates the method used in calculations of heat flow values. For details, see the text.

The new heat flow map for the Antarctic region is illustrated in Figure 6. Note that the region of Antarctic peninsula is characterized by heat flow values in excess of 80mW/m^2. It appears to be continuation of high heat flow belt in the southwestern parts of the Andean magmatic belt (Vieira and Hamza, 2019). The belt of moderately high heat flow continues to the south of Antarctic peninsula in areas of subglacial lakes. This is a consequence of the fact that thermal regime above the subglacial lakes require heat fluxes of more than 60 mW/m^2 to maintain basal ice at the pressure-melting point.

The practice of inserting representative theoretical values to fill gaps in observational data sets is similar to that adopted in deriving global heat flow maps (Hamza et al, 2008; Davies and Davies, 2010; Vieira and Hamza, 2018). On the other hand, large parts of the eastern Antarctic region are characterized by heat flow values lower than the global mean. This observation is in general agreement with those observed for Precambrian cratonic regions. In the interior parts of eastern Antarctica areas with heat flow less than 50mW/m^2 seem to occur along a north south trending belt. The separation between low and high heat flow belts occur along the position of Transantarctic Mountains.

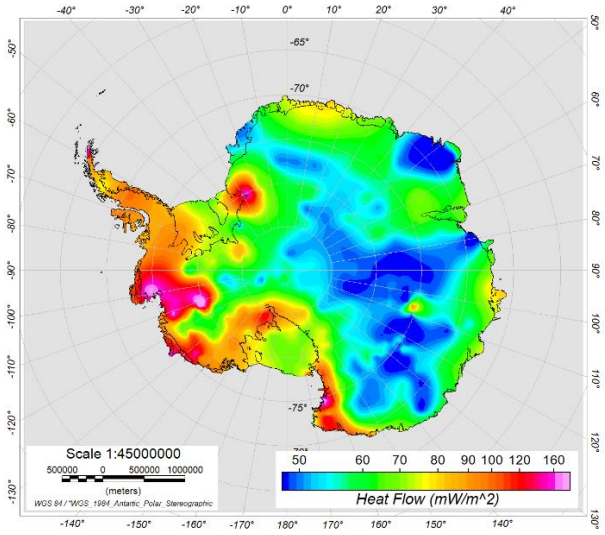

Figure 6 – New heat flow map of Antarctica based on revised data sets. For details, see the text.

5. Conclusions

The present work provides a new look into the nature and distribution of terrestrial heat flow in the Antarctic continent, based on recent advances in data analysis and regional assessments. The datasets considered include that compiled by the global data base of IHFC, inferences based on volcanic settings and estimates that rely on basal temperatures of glaciers in localities that are known to host subglacial lakes. Most heat flow values reported in the present work are in reasonable agreement with results discussed in several previous studies (e.g. Begelman et al., 2017; Carson et al., 2014; Dziadek et al., 2017; Engelhardt, 2004; Fisher et al., 2015; Risk and Hochstein, 1974; Salamatin et al., 1998; Schröeder et al., 2014).

The high heat flux in areas of subglacial lakes appears to be a consequence of active hydrological systems believed to be operating beneath the glaciers. The eastern region is characterized by relatively low heat flow values in the range of 30–60 mW/m^2, as expected for dominantly cratonic regions. This observation appears to be in general agreement with the Curie depth values derived from spectral analysis magnetic survey data. The major features in the new heat flow map of the present work reveal striking agreement with conclusions of An et al. (2015), based on seismic velocities.

The new heat flow map is believed to have potential implications not only in studies of regional tectonics, but also in a better understanding of geothermal systems operating beneath subglacial lakes.

6. Acknowledgments

This study is part of post-doctoral project of the first author (PNPD) at the Department of Geophysics of the National Observatory - ON/MCTI. The third author is recipient of a research scholarship (Process No. 306755/2017-3) granted by the National Research Council of Brazil (CNPq).

References

An, M., Wiens, D.A., Zhao, Y., Feng, M., Nyblade, A.A., Kanao, M., Li, Y., Maggi, A., Lévêque, J., 2015. Temperature, lithosphere-asthenosphere boundary, and heat flux beneath the Antarctic Plate inferred from seismic velocities. JGR: Solid Earth, 120, 8720-8742.

Annen, C., Scaillet, B., Sparks, R.S.J., 2006. Thermal constraints on the emplacement rate of a large intrusive complex: the Manaslu Leucogranite, Nepal Himalaya. Journal of Petrology, 47, 71-95.

Begelman, C.B., Slawek, T., Fisher, A.T., 2017. Spatially variable geothermal heat flux in West Antarctica: evidence and implications, Geophysical Research Letters, 44(19), 9823-9832.

Carslaw, H.S., Jaeger, J.C., 1959. Conduction of heat in solids. Clarendon Press.

Carson, C.J., McLaren, S.J., Roberts, L., Boger, S.D. Blankenship, D.D., 2014. Hot rocks in a cold place: high sub-glacial heat flow in East Antarctica, Journal of the Geological Society, 171(1), 9–12.

Davies. J.H., Davies D.R. 2010. Earth´s surface heat flux. Solid Earth, 1. p. 5-24.

Dalziel, I.W.D., Elliot, D.H., 1982. West Antarctica – problem child of Gondwanaland. Tectonics, 1, 3–19.

Dziadek, R., Gohl, K., Diehl, A., Kaul, N. 2017. Geothermal heat flux in the Amundsen Sea sector of West Antarctica: New insights from temperature measurements, depth to the bottom of the magnetic source estimation, and thermal modeling. Geochemistry, Geophysics, Geosystems, 18(7), 2657-2672.

EarthHow, 2019. A Guide to the Magnetosphere, https://earthhow.com/magnetosphere/ (Accessed January 4, 2020).

Engelhardt, H., 2004. Ice temperature and high geothermal flux at Siple Dome, West Antarctica, from borehole measurements. Journal of Glaciology, 50 (169), 251–256.

Fedorov, L.V., Grikurov, G.E., Kurinin, R.G., Masolov, V.N. 1982. Crustal structure of the Lambert Glacier area from geophysical data. In: Craddock, C. (ed.) Antarctic Geoscience. University of Wisconsin Press, Madison, WI, 931–936.

Fisher, A.T., Mankoff, K.D., Tulaczyk, S.M., Tyler, S.W., Foley, N., Team, W.S., 2015. High geothermal heat flux measured below the West Antarctic Ice Sheet, Science Advances, 1(6), e1500093.

Goodge, J.W., 2002. From Rodinia to Gondwana: supercontinent evolution in the Transantarctic Mountains. In: Gamble, J.A., Skinner, D.N.B., Henrys, S. (eds) Antarctica at the Close of a Millennium. Royal Society of New Zealand, Bulletin, 35, 61–74.

Goodge, J.W., 2018. Crustal heat production and estimate of terrestrial heat flow in central East Antarctica, with implications for thermal input to the East Antarctic ice sheet. The Cryosphere, 12, 491-504.

Hamza V.M., Cardoso R.R., Ponte Neto, C.F., 2008. Spherical Harmonic Analysis of Earth's Conductive Heat Flow. International Journal of Earth Sciences, 97, 205-226.

Harley, S. L., Fitzsimons, I. C., Zhao, Y. 2013. Antarctica and supercontinent evolution: historical perspectives, recent advances and unresolved issues. Geological Society, 383(1), 1-34.

IHFC, 2009. The global heat flow database provided by the international heat flow commission (IHFC). Available at http://www.heatflow.und.edu,last updated June 10, 2009.

Iyer, S.S., Hamza, V.M., 2019. Paleo heat flow in areas of Sedimentary Exhalative (SEDEX) deposits of Eastern Brazil. International Journal of Terrestrial Heat Flow and Applied Geothermics, 2, 11-16.

LeMasurier, W. E., Thomson, J. W., Baker, P.E., Kyle, P.R., Rowley, P.D., Smellie, J.L., Verwoerd, W.J. 1990. Volcanoes of the Antarctic Plate and Southern Ocean (Vol. 48). American Geophysical Union, 487pp. (Antartic Research Series, 48).

Lisker, F., Brown, R. & Fabel, D. 2003. Denudational and thermal history along a transect across the Lambert Graben, northern Prince Charles Mountains, Antarctica, derived from apatite fission track thermochronology. Tectonics, 22, 1001 - 1014, http://dx.doi.org/10.1029/2002TC001477.

Martos, Y.M., Catalán, M., Jordan, T.A., Golynsky, A., Golynsky, D., Eagles, G., Vaughan, D.G. (2017). Heat flux distribution of Antarctica unveiled. Geophysical Research Letters, 44(22), 11-417.

Morin, R.H., Williams, T., Henrys, S.A., Magens, D., Niessen, F., Hansaraj, D. 2010. Heat flow and hydrologic characteristics at the AND-1B borehole, ANDRILL McMurdo Ice Shelf Project, Antarctica. Geosphere, 6(4), 370 - 378.

Noguchi, T., 1970. An attempted evaluation of geothermal energy in Japan. Geothermics, 2, 474-477.

Phillips, G., Laufer, A.L., 2009. Brittle deformation relating to the Carboniferous–Cretaceous evolution of the Lambert Graben, East Antarctica: a precursor for Cenozoic relief development in an intraplate and glaciated region. Tectonophysics, 471, 216–224

Risk, G.F., Hochstein, M.P., 1974. Heat flow at arrival heights, Ross Island, Antarctica. New Zealand Journal of Geology and Geophysics, 17, 629 - 644.

Robin, G. de Q., 1955. Ice movement and temperature distribution in glaciers and ice sheets. J. Glaciology, 3, 589–606.

Robin, G. De Q., Swithinbank, C.W.M., Smith, B.M.E., 1970. Radio echo exploration of the Antarctic ice sheet. International Association Scientific Hydrology Publication, 86, 97 – 115.

Salamatin, A.N., Lipenkov, V.Y., Barkov, N.I., Jouzel, J., Petit, J.R., Raynaud, D., 1998. Ice core age dating and paleothermometer calibration based on isotope and temperature profiles from deep boreholes at Vostok Station (East Antarctica). Journal of Geophysical Research, 103(D8), 8963–8977.

Schroeder, D.M., Blankenship, D.D., Young, D.A., Quartini, E., 2014. Evidence for elevated and spatially variable geothermal flux beneath the West Antarctic Ice Sheet, Proceedings of the National Academy of Sciences, 111(25), 9070-9072.

Siegert, M.J., Carter, S., Tabacco, I., Popov, S., Blankenship, D.D., 2005. A revised inventory of Antarctic subglacial lakes. Antarctic Science, 17, 453–460.

Smith, R.L., Shaw, H.R., 1978. Igneous-related geothermal systems. Assessment of geothermal resources of the United States, 12-17.

Stump, E., 1995. The Ross Orogen of the Transantarctic Mountains. Cambridge University Press, Cambridge.

Suarez, T.A. 2017. Cooling of intrusive bodies in the interior of continental crust: effects of the release of latent heat (in Portuguese). Unpublished M.Sc. Thesis, University of Sao Paulo, São Paulo (Brazil). 88p.

Vaughan, A.P.M., Leat, P.T., Pankhurst, R.J., 2005. Terrane processes at the margins of Gondwana: introduction. In: Vaughan, A.P.M., Leat, P.T., Pankhurst, R.J. (eds) Terrane Processes at the Margin of Gondwana. Geological Society, London, Special Publications, 246, 1–21.

Van Liefferinge, B., Pattyn, F., 2013. Using ice-flow models to evaluate potential sites of million-year-old ice in Antarctica. Climate of the Past Discussions, 9(3).

Vieira, F.P., Hamza, V.M., 2018. Global Heat Flow: New Estimates Using Digital Maps and GIS Techniques. International Journal of Terrestrial Heat Flow and Applied Geothermics, 1, 6-13.

Vieira, F.P., Hamza, V.M., 2019. Assessment of Geothermal Resources of South America - A New Look. International Journal of Terrestrial Heat Flow and Applied Geothermics, 2, 46 - 57.

Wright, A., Siegert, M. 2012. A fourth inventory of Antarctic subglacial lakes. Antarctic Science, 24(6), 659 - 664.

Appendix

Heat flow data for 306 localities based on basal temperatures of glaciers in the Antarctic region, with values higher than the global mean of 65mW/m²(Vieira and Hamza, 2018). (GT – Glacier thickness; q – Heat Flow)

Locality	Long	Lat	GT (m)	q (mW/m²)
MacAyeal4	227.34	-78.68	2094	65
Academy8	307.07	-85.65	2064	65
Bindschadler2	229.80	-79.94	2105	65
Recovery5	350.39	-81.28	2054	65
Recovery6	352.76	-81.43	2092	65
CookW1	149.71	-69.66	2097	65
Bindschadler2	229.80	-79.94	2105	65
Bindschadler3	233.35	-80.03	2129	64
Byrd2	146.89	-80.68	2161	64
Recovery7	354.02	-81.64	2141	64
Bindschadler4	234.43	-80.73	2178	63
Bindschadler6	237.37	-80.57	2189	63
Kamb7	236.56	-81.92	2243	63
M-2710	39.89	-73.42	2180	63
Sovetskaya	88.50	-78.10	4200	45
Lake Vostok	104.50	-78.15	3945	47
SI-3	124.80	-76.57	3621	49
SI-4	157.28	-73.28	2827	56
SI-5	119.27	-77.20	3835	48
Concordia Lake	125.02	-74.07	4055	46
SI-7	-150.00	-88.30	2807	56
SI-8	123.94	-72.31	3254	52
SI-9/16/20	129.70	-76.80	3410	51
SI-10	127.41	-75.94	3449	50
SI-11/ITL-7	126.56	-75.81	3634	49
SI-12	125.60	-75.65	3399	51
SI-13/14/ITL-10	122.66	-75.84	3427	50
SI-15	126.98	-75.14	3447	50
SI-17	119.54	-73.45	3924	47
Adven. Trench	135.34	-76.24	3780	48
SI-19	148.27	-79.93	2333	61
SI-21	128.90	-74.91	3890	47
SI-22	124.95	-75.97	3168	52
SI-23	125.97	-75.78	3162	52
SI-24	126.48	-75.69	3650	49
SI-25/76	124.70	-74.97	3045	54
SI-26	120.39	-75.61	3057	53
SI-27	126.90	-73.40	4010	47
SI-28/63	128.35	-73.17	4050	46
SI-29	140.95	-69.71	2269	62
SI-30/58	136.87	-68.44	4117	46
SI-31	129.03	-75.82	3069	53
SI-32	126.03	-76.40	3500	50
SI-33	118.50	-74.03	4084	46
Aurora Lake	119.37	-74.46	4066	46
SI-35	126.30	-77.12	3741	48
SI-36	128.35	-71.81	2994	54
SI-37	128.20	-71.79	3021	54
SI-38	139.92	-74.04	3285	51
SI-39	148.86	-75.73	3010	54
SI-40	120.00	-88.50	3100	53
SI-41	75.00	-87.00	2943	54
SI-42/43	125.18	-76.19	3884	47
SI-44	133.47	-81.84	2641	58
SI-46	100.40	-77.40	3709	48
SI-47	97.50	-76.80	3715	48
SI-48	64.52	-88.73	2997	54
SI-49	70.54	-88.36	3027	54
SI-50	112.68	-88.37	3068	53
SI-51	148.62	-87.61	3062	53
SI-52	136.88	-88.71	3070	53
SI-53	144.50	-88.42	2741	56
SI-54/59	92.50	-77.10	3784	48
SI-55	99.00	-78.00	3399	51
SI-56	155.68	-71.13	2347	61
SI-57	151.60	-70.47	2418	60
SI-60	93.50	-76.80	3426	50
SI-61	144.30	-79.15	2580	58
SI-62	129.41	-72.74	3828	48
SI-64	119.71	-75.76	3574	49
SI-65	118.11	-76.07	3733	48
SI-66	118.60	-78.00	3341	51
SI-67	246.50	-79.09	2700	57
SI-68	261.05	-82.06	2894	55
SI-69	67.73	-79.04	2500	59
SI-70 - Pole	198.44	-89.97	2857	55
SI-71	265.08	-82.99	3200	52
SI-72	253.83	-86.36	2814	56
SI-73	254.44	-86.43	2906	55
SI-74	248.74	-86.77	3960	47
SI-75	234.70	-87.77	2315	62
SI-77	124.19	-74.92	3925	47
Ellsworth	269.43	-78.99	3400	51
ITL-1	121.63	-75.46	3570	49
ITL-2	121.61	-75.62	3513	50
ITL-3	122.31	-75.42	3030	54
ITL-4	122.28	-74.78	3769	48
ITL-5	125.02	-75.34	3150	53
ITL 6	126.03	-75.95	2975	54
ITL 8	121.73	-74.91	3416	50
ITL 9	125.92	-75.02	3461	50
ITL 11	117.67	-75.61	4457	44
ITL 12	116.42	-74.67	4155	46
ITL 13	116.94	-74.88	4460	44
Vincennes Lake	127.94	-74.16	4028	46
ITL 17	119.71	-73.70	4034	46
ITL 18	115.19	-77.63	3500	50
M-310	26.94	-74.30	2427	60
M-511	14.47	-80.90	2340	61
M-511	27.29	-75.17	2770	56
M-610	33.09	-75.74	2560	58
M-2011	37.43	-77.50	3125	53
M-2713	27.03	-75.46	2830	56
M-3112	44.46	-77.70	2860	55
M-3710	32.62	-77.96	3070	53
M-3010	77.89	-82.34	3575	49
M-3510	62.73	-77.96	2834	56
M-3112	45.77	-77.70	2640	58
M-3809	43.70	-77.24	3130	53
M-3211	56.77	-72.10	2535	59
SAE35	45.82	-80.30	3240	52
WLK-6	144.66	-77.10	3413	50
WLK-14	145.09	-76.71	3503	50
WLK-12	144.29	-76.43	3547	50
WLK-24	144.75	-76.12	3557	49

WLK-17	126.41	-75.09	3480	50
DCSx/X02b X02e	139.23	-80.41	3059	53
DCS/DCSx/X01c	120.08	-81.84	2933	55
DCS/DCSx/X01d	137.54	-80.65	2981	54
LVS-12	117.99	-75.85	4661	43
LVS-9	88.87	-79.30	3890	47
LVS-13	91.43	-77.98	3787	48
90ºE lake	91.08	-77.38	4074	46
C25SAE1	94.57	-76.75	3500	50
C25SAE2	94.83	-77.08	3560	49
Bindschadler5	236.01	-80.61	2242	63
Kamb10	239.87	-81.45	2393	60
L1	133.27	-74.00	4200	45
U1	135.00	-75.94	3933	47
U2	135.77	-76.34	3231	52
U3	135.93	-76.68	2687	57
No name 1	107.13	-78.58	3635	49
No name 2	103.72	-77.23	3720	48
No name 3	107.53	-77.85	2915	55
No name 4	107.26	-77.47	3515	50
No name 5	107.01	-77.30	3435	50
No name 6	107.01	-77.20	3305	51
LVS-8	106.69	-76.94	3540	50
No name 7	106.02	-76.66	3735	48
No name 8	106.02	-76.60	3400	51
No name 9	104.59	-78.32	3605	49
No name 10	107.35	-78.08	3295	51
No name 11	107.80	-78.05	3345	51
No name 12	107.51	-77.67	2740	56
No name 13	107.51	-77.60	3135	53
No name 14	107.51	-77.58	3100	53
No name 15	103.98	-77.97	3280	52
No name 16	105.37	-78.60	3600	49
No name 17	105.86	-78.66	3320	51
No name 18	103.62	-77.88	3650	49
No name 19	103.76	-77.80	3740	48
No name 20	101.96	-76.91	3715	48
No name 21	101.43	-76.70	3835	48
No name 22	101.74	-76.29	3720	48
No name 23	104.30	-78.12	3190	52
LVS-11	106.51	-77.25	3740	48
No name 24	103.36	-77.50	3720	48
No name 25	103.86	-75.91	3770	48
No name 26	104.99	-78.58	3880	47
No name 27	105.59	-78.53	3740	48
Komsomolskoe	97.29	-73.62	3590	49
Pionerskoe Lake	95.54	-69.75	2400	60
WLK-4	150.11	-77.42	2686	57
WLK-5	148.93	-76.87	2990	54
WLK-7	153.71	-77.16	2712	57
WLK-8	150.94	-76.99	2942	54
WLK-9	150.02	-77.19	2774	56
WLK-10	150.21	-76.88	3018	54
WLK-11	147.75	-77.32	3025	54
WLK-13	139.04	-75.76	2873	55
Horse (WLK-15)	126.59	-75.23	3375	51
WLK-16	126.28	-74.57	3697	48
WLK-18	127.56	-74.89	3510	50
WLK-19	137.35	-76.02	2985	54
WLK-21	126.84	-75.43	3488	50
WLK-22	136.88	-76.23	2906	55
WLK-23	137.33	-76.12	2969	54
WLK-26	132.37	-76.00	2703	57
WLK-27	135.75	-75.65	3442	50
WLK-28	137.95	-76.37	2612	58
WLK-29	143.81	-76.15	3400	51
WLK-30	146.04	-76.49	3399	51
WLK-31	138.74	-76.57	2622	58
WLK-32	138.46	-76.59	2616	58
WLK-33	147.24	-77.29	3062	53
WLK-34	148.30	-76.80	3175	52
WLK-35	150.14	-76.67	3037	54
WLK-36	149.68	-76.99	2947	54
WLK-37	150.47	-76.49	3050	53
WLK-38	150.61	-77.08	2900	55
WLK-39	150.92	-76.90	2917	55
WLK-40	150.92	-77.28	2743	56
WLK-41	151.78	-77.12	2778	56
WLK-42	152.49	-77.31	2855	55
LVS-1	119.23	-75.60	4095	46
LVS-2	89.79	-78.66	3706	48

LVS-3	118.71	-75.71	3867	47
LVS-4	103.32	-77.46	3664	49
LVS-5	103.30	-77.68	3623	49
LVS-6	108.16	-78.02	3306	51
LVS-14	102.10	-77.06	3229	52
PPT-1	-143.83	-89.76	2866	55
PPT-2	-120.39	-88.91	3095	53
PPT-3	-86.10	-89.85	2784	56
PPT-12	30.04	-89.90	2888	55
PPT-17	-13.77	-89.48	2911	55
PPT-18	2.28	-88.47	3241	52
PPT-19	-150.01	-89.21	2809	56
PPT-20	-149.24	-88.92	2113	64
PPT-21	-141.19	-89.41	2476	59
PPT-22	-140.85	-88.31	3002	54
PPT-23	-139.78	-88.49	2990	54
PPT-25	-111.22	-89.57	3015	54
PPT-26	-126.29	-89.33	3032	54
PPT-28	-103.87	-89.61	2972	54
PPT-29	-21.36	-89.43	2827	56
PPT-30	-49.28	-89.45	2959	54
PPT-31	-128.95	-88.50	2871	55
PPT-32	-78.70	-89.34	2927	55
PPT-35	7.60	-88.26	3688	49
PPT-36	-83.34	-89.32	2879	55
PPT-37	-58.47	-89.24	2870	55
PPT-38	-13.71	-88.96	2684	57
PPT-39	-78.86	-89.17	3090	53
PPT-40	-117.81	-88.41	2742	56
PPT-41	-110.58	-88.61	3067	53
PPT-42	-80.29	-89.04	2821	56
PPT-43	-116.89	-88.36	2768	56
PPT-44	-43.83	-89.04	2989	54
Recovery A	14.28	-82.40	3500	50
Recovery B	18.13	-82.85	3500	50
Recovery C	21.37	-84.31	2687	57
Recovery D	21.61	-84.99	3100	53
ITL-19	121.56	-75.03	3187	52
ITL-20	119.85	-75.06	3375	51
ITL-21	121.44	-74.85	3312	51
ITL-22	122.17	-75.02	3062	53
ITL-23	120.15	-74.07	3875	47
ITL-24	128.00	-76.17	2936	55
ITL-25	127.19	-76.15	2881	55
ITL-26	126.69	-76.13	2856	55
ITL-27	126.56	-76.13	2910	55
ITL-28	125.06	-76.07	4300	45
Academy9	307.77	-85.86	2174	64
Academy10	309.00	-85.77	2356	61
Academy11	311.59	-85.80	2595	58
Academy12	314.62	-85.71	2658	57
Academy13	317.59	-85.64	2710	57
Academy14	320.43	-85.78	2559	58
Academy15	322.31	-86.02	2453	60
Academy16	324.30	-85.99	2364	61
ByrdS4	143.71	-80.75	2533	59
ByrdS5	143.38	-80.58	2726	57
ByrdS6	143.66	-80.32	2466	60
ByrdS7	143.74	-80.03	2612	58
ByrdS8	142.41	-80.01	2695	57
ByrdS9	142.30	-81.47	2389	61
ByrdS10	139.03	-81.83	2467	60
ByrdS11	138.59	-81.47	2750	56
ByrdS12	138.24	-80.90	2741	56
ByrdS13	142.83	-78.93	2860	55
ByrdS14	139.78	-78.83	2903	55
ByrdS15	138.96	-78.81	2903	55
CookE1	155.34	-71.87	2766	56
CookE2	155.79	-72.80	2679	57
CookW2	149.38	-70.84	2781	56
David3	152.92	-75.24	2299	62
David4	152.25	-75.73	2144	64
David5	152.46	-74.88	2273	62
David6	145.24	-75.39	3320	51
EAP1	140.64	-85.84	2728	57
EAP2	135.48	-85.68	2772	56
EAP3	132.79	-85.90	2952	54
EAP4	128.37	-85.91	3032	54
EAP5	124.42	-85.66	2904	55
EAP6	104.04	-85.49	3190	52
EAP7	122.44	-83.97	3315	51

EAP8	109.85	-75.19	3612	49
EAP9	135.56	-75.81	3584	49
Kamb11	239.86	-81.25	2489	59
Kamb12	242.92	-80.85	2847	55
Mulock1	149.11	-78.09	2766	56
Ninnis1	144.27	-70.89	3169	52
Nimrod2	141.00	-84.32	3300	51
Recovery7	354.02	-81.64	2141	64
Recovery8	355.88	-81.80	2250	62
Recovery9	2.33	-82.91	2375	61
Recovery10	5.94	-83.50	2455	60
Recovery11	8.42	-81.72	2651	57
Totten1	107.50	-70.10	2455	60
Totten2	110.51	-70.83	3942	47
Vostok1	106.83	-77.17	3739	48
Whillans8	246.40	-83.50	2784	56
Wilkes1	106.71	-68.81	3245	52
Wlikes2	121.57	-68.70	2132	64
R03Wa_1	130.40	-70.43	3910	47
R04Ea_9	135.00	-71.62	2790	56
R05Ea_4	128.12	-71.67	3284	51
R05Ea_5	129.05	-71.84	3750	48
R06Wa_4	127.04	-72.88	3869	47
R07Ea_9	126.02	-73.44	3707	48
R07Ta_1	125.65	-73.81	3644	49
R08Wa_0.1	122.58	-74.29	3745	48
R08Wa_0.2	122.50	-74.30	3709	48
R13Ea_8	106.04	-75.98	3521	50
R15Ea_4	100.82	-74.08	3523	50
Byrd2	146.89	-80.68	2161	64